

Isolation, Sequence Identification and Tissue Expression of a Novel Tobacco (*Nicotiana tabacum*) Gene-TBG1

Nian Fuzhao¹, Zhang Yonghui², Su Xiangyun³, Zou Juqiu³, Zhao Leifeng^{*1}

¹College of Tobacco Science, Yunnan Agricultural University, Kunming 650201, China

²Technological Center of Tobacco Company of Sichuan Province, Luzhou 646000, China

³Feedstock Supply Department of Industrial Limited-Liability Company of Chinese Tobacco Company of Hunan province, Changsha 410014, China

*fuzhaonian@126.com

Abstract

The complete coding sequence of one tobacco (*nicotiana tabacum*) gene- β -galactosidase precursor (*TBG1*), was amplified based on some tobacco ESTs. The complete coding sequence of tobacco *TBG1* gene was 2,526 bp which encodes a protein of 841 amino acids. Sequence analysis revealed that the *TBG1* of tobacco shares high homology with the *TBG1* of *lycopersicon esculentum* (91%), cacao (81%), castor bean (81%) and papaya (81%). Results also showed that tobacco *TBG1* gene has a closer genetic relationship with the *TBG1* gene of *lycopersicon esculentum*. The expression profile was studied and the results indicated that tobacco *TBG1* gene was differentially expressed in detected tobacco tissues including leaf, stem, root and flower. Our experiment established the foundation for further research on this tobacco gene.

Keywords

Tobacco; *TBG1*; Tissue Expression

Introduction

β -galactosidases are thought to be responsible for the conspicuous reduction in the level of galactosyl residues which occurs in many ripening fruits. These enzymes have also been detected in a wide range of plant organs and tissues undergoing developmental changes such as seeds, cotyledons, elongating epicotyls, and in freshly harvested asparagus spears. So far, only exo-acting activities have been found in plants and these enzymes are characterized by their ability to hydrolyse terminal non-reducing β -d-galactosyl residues from β -d-galactosides. They are usually assayed by their ability to release galactosyl residues from artificial substrates such as p-nitrophenyl- β -d-galactopyranoside, 4-methyl umbelliferyl- β -d-galactopyranoside and X-gal. In many cases, however, their natural substrates are unknown, but probably include chloroplast galactolipids as well as cell wall galactans (Gross and Sams, 1984; MS,

1994; Carey *et al.* 1995; Smith *et al.* 1998; Smith and Gross, 2000; Carey *et al.* 2001; Shlush *et al.* 2013; Fonseca-Berzal *et al.* 2013; Choi *et al.* 2013).

Although β -galactosidases play important roles in biological processes of plants, until today, the tobacco β -galactosidase precursor (*TBG1*) gene has not been reported yet. In present experiment, we would isolate the complete mRNA sequence of tobacco *TBG1* gene, subsequently perform some necessary sequence analysis and tissue expression analysis for this gene; thus the primary foundation of understanding this tobacco gene was established.

Materials and Methods

Samples Collection, RNA Extraction and First-strand cDNA Synthesis

Tobacco plants (Chinese local variety Yunyan 85) were grown in a naturally lit glasshouse with normal irrigation and fertilization. The tissues including leave, stem, root, flower were harvested and immediately frozen in liquid nitrogen and stored at -80°C . Total RNA extraction and first-strand cDNA synthesis for these tissue samples were performed as the methods described by Li *et al.* (2008).

Isolation of the Coding Sequence

RT-PCR was performed to amplify complete coding sequences of tobacco *TBG1* gene using the cDNA obtained from the pooled tissues above. The 20 μl reaction system was: 2.0 μl cDNA, 2.0 μl 2 mM mixed dNTPs, 2.0 μl 10 \times Taq DNA polymerase buffer, 1.2 μl 25 mM MgCl₂, 1.0 μl 10 mM forward primer, 1.0 μl 10 mM reverse primer, 2.0 units of Taq DNA polymerase (1 U/1 μl), and 9.8 μl sterile water. The primers for tobacco *TBG1* gene isolation were designed based on

the tobacco EST sequences (GeneBank numbers: FS390322, FG200071, FG192756, FG191482, FG164696 and EB678821) which were highly homologues with the coding sequence of TBG1 gene of lycopersicon esculentum(TABLE 1). The PCR program initially started with a 94°C denaturation for 4 min, followed by 35 cycles of 94°C/1 min, 56°C (TABLE 1)/1 min, 72°C /1 min, then 72°C extension for 10 min, finally 4°C to terminate the reaction. Every PCR was repeated five times. The PCR product was then cloned into PMD18-T vector and sequenced bidirectionally with the commercial fluorometric method. At least five independent clones were sequenced.

TABLE 1 RT-PCR PRIMERS FOR TOBACCO TBG1 GENE AND ANNEALING TEMPERATURE

| Gene | Primer sequence | Ta/ °C | Length/(bp) |
|------|---|--------|-------------|
| TBG1 | Forward 1: 5'- ATGGATTGTTCTTGGATTGC-3' | 56 | 2526 |
| | Reverse 1: 5'- TCAGCTGCAAACAACCTC-3' | | |
| | | | |

TABLE 2 QRT-PCR PRIMERS FOR TOBACCO TBG1, ACTIN GENES AND ANNEALING TEMPERATURE

| Gene | Primer sequence | Ta/ °C | Length/(bp) |
|-------|--|--------|-------------|
| TBG1 | Forward 2: 5'- AGAAGGAGGAGTGGATGT-3' | 56 | 224 |
| | Reverse 2: 5'- TGAAACTGATACCTGGAAC-3' | | |
| | Forward 3: 5'- CCATTCTTCGTTTGGACCTT -3' | | |
| Actin | Reverse 3: 5'- TTCTGGGCAACGGAACCT-3' | 56 | 257 |
| | | | |

Quantitative Real Time PCR (qRT-PCR) for Tissue Expression Profile Analysis

qRT-PCR for evaluating the level of mRNA for TBG1 gene was performed on the ABI Prism 7300 Sequence Detection Systems (Applied Biosystems, Foster City, CA, USA). PCR reactions for each sample were carried out in 25 µl reaction volume containing 1µl SYBR Green real-time PCR Master Mix, 100 ng cDNA template and 200 nM each primer. Conditions for real-time PCR were: an initial denaturation at 95°C for 3 min, 40 cycles of 95°C for 15 s, optimal annealing temperature for each specific primer for 15 s (TABLE 2), 72°C for 20 s. For each sample, reactions were set up in triplicate to ensure the reproducibility of the results. The gene relative expression levels were quantified relative to the expression of the reference gene, actin (GenBank Accession No. GQ339768), by employing the 2^{-ΔΔCt} value model (Livak and Schmittgen TD, 2001).

Sequence Analysis

The cDNA sequence prediction was conducted using GenScan software (<http://genes.mit.edu/GENSCAN.html>). The protein prediction and analysis were performed using the Conserved Domain Architecture Retrieval Tool of BLAST at the National Center for Biotechnology Information (NCBI) server (<http://www.ncbi.nlm.nih.gov/BLAST>) and the Clustalw software (<http://www.ebi.ac.uk/clustalw>).

```

Common tobacco      --MDCSWIAMWNVLLILLVLLSSWVSCGSIASVSYDHKAIIVNGQRKILIS
Lycopersicon esculentum  -----MGCTLIILMLNVLLVLLGSWVFSGTASVSYDHRRAIIVNGQRRILIS
Cacao                --MDSNSKLPVMWNALLVLLFASWVCSVSASVSYDRKAITINGQRRILIS
Castor bean          MKKLIIMRNIDNNNILVVFLLGLWVCSVSSSVSYDSKAITINGQRRILIS
Papaya               -----MNVILAAVLVSSLLVSVIASVSYDHKAITINGKRRILLIS
                    : : * . . : . : * * * * * : * * * * *
Common tobacco      GSIHYPRSIPEMWPDLIQKAKEGGVDVIQTYVFWNGHESEEGKYFFEGRY
Lycopersicon esculentum  GSVHYPRSTPEMWPGLIIQKAKEGGVDVIQTYVFWNGHEPQQGKYFFEGRY
Cacao                GSIHYPRSSPEMWPDLVQKAKEGGLDVIQTYVFWNGHEPAPGKYFFQGN
Castor bean          GSIHYPRSSPEMWPDLIQKAKEGGLDVIQTYVFWNGHEPSPGKYFFEGNY
Papaya               GSIHYPRSTPEMWPDLIQKAKEGGLDVIQTYVFWNGHEPSPGKYFFGGNY
                    ** : * * * * * : * * * * * : * * * * * : * * * * *
Common tobacco      DLVKFIKVVQEAGLYVHLRIGPYACAENWFSGFPVWLKYVPGISFRDNE
Lycopersicon esculentum  DLVKFIKLVHQAGLYVHLRVGPYACAENWFSGFPVWLKYVPGISFRDNG
Cacao                DLVKFIKLVQAGLYVHLRIGPYVCAENWFSGFPVWLKYIPGINFRDNG
Castor bean          DLVKFIKLVKQAGLYVHLRIGPYVCAENWFSGFPVWLKYVPGINFRDNG
Papaya               DLVRFIKLVKQAGLYVHLRIGPYVCAENWFSGFPVWLKYIPGIAFRDNG
                    *** : * * * * * : * * * * * : * * * * * : * * * * *
Common tobacco      PFKAAMQKFTTKIVDMMKSERLYQSQGGPIILSQIENEYGPMEWELGEPG
Lycopersicon esculentum  PFKAAMQKFTAKIVNMMKAERLYETQGGPIILSQIENEYGPMEWELGAPG
Cacao                PFKAQMQRFTTEKIVDMMKAEERLFESQGGPIILSQIENEYGPMEYELGAPG
Castor bean          PFKAQMQRFTTKIVNMMKAERLFESQGGPIILSQIENEYGPMEYELGAPG
Papaya               PFKAYMQRFTTKIVDMMKAEGLFESQGGPIILSQIENEYGPMEYELGAAG
                    *** : * * * * * : * * * * * : * * * * * : * * * * *
Common tobacco      KAYSEWAAKMAVDLGTGVPWIMCKQDDVPDPIINTCNGFYCDYFLPNKAN
Lycopersicon esculentum  KSYAQWAAKMAVGLDTGVPWVMCKQDDAPDPIINACNGFYCDYFSPNKAY
Cacao                KAYTDWAAKMAVGLGTGVPWVMCKQDDAPDPIINTCNGFYCDYFSPNKAY
Castor bean          QAYSQWAAKMAVGLGTGVPWVMCKQDDAPDPIINTCNGFYCDYFSPNKPY
Papaya               RAYSQWAAQMAVGLGTGVPWVMCKQDDAPDPIINSCNGFYCDYFSPNKAY
                    : : * * * * * : * * * * * : * * * * * : * * * * *
    
```

| | |
|-------------------------|--|
| Common tobacco | KPKMWTEAWTAWFTEFGGVPVYRPAEDMAFAVARFIQIGGSFVNYMYHG |
| Lycopersicon esculentum | KPKIWEAWTAWFTGFGNPVYRPAEDLAFSVAKFIQKGGSFINYMYHG |
| Cacao | KPKIWEAWTGWYTEFGGAVPYRPAEDLAFSVAKFIQKGGAFINYMYHG |
| Castor bean | KPKMWTEAWTGWFTFEGGAVPYRPAEDLAFSVAKFIQKGGAFINYMYHG |
| Papaya | KPKMWTEAWTGWFTFEGGAVPYRPAEDLAFSVAKFIQKGGSFINYMYHG ***:*****.*:* **..*****.***:***:***.*:*:***** |
| | |
| Common tobacco | GTNFGRTAGGPFPIATSYDYDAPLDEFGLLRQPKWGHKDLHRAIKLCEPA |
| Lycopersicon esculentum | GTNFGRTAGGPFPIATSYDYDAPLDEYGLLRQPKWGHKDLHRAIKLCEPA |
| Cacao | GTNFGRTAGGPFPIATSYDYDAPLDEYGLLRQPKWGHKDLHRAIKLCEPA |
| Castor bean | GTNFGRTAGGPFPIATSYDYDAPLDEYGLLRQPKWGHKDLHRAIKLCEPA |
| Papaya | GTNFGRTAGGPFPIATSYDYDAPLDEYGLVRQPKWGHKDLHRAIKLCEPA *****:*****:***:*****:***:*****:***:*****:***:***** |
| | |
| Common tobacco | LVSADPIVTPGLGNYQEAVFKSESGACAAFLANYNQHSFAKVAFGNMHYN |
| Lycopersicon esculentum | LVSADPIVTPGLGNYQEAVFKSESGACAAFLANYNQHSFAKVAFGNMHYN |
| Cacao | LVSADPIVTPGLGNYQEAVFKSESGACAAFLANYNQHSFAKVAFGNMHYN |
| Castor bean | LVSADPIVTPGLGNYQEAVFKSESGACAAFLANYNQHSFAKVAFGNMHYN |
| Papaya | LVSADPIVTPGLGNYQEAVFKSESGACAAFLANYNQHSFAKVAFGNMHYN **.. * * ** .***:***: : * *****: :***:***.* ** |
| | |
| Common tobacco | LPPWSISILPDCKNTVFNTARIGAQSAQMKMTSVSRG--FSWDSFNEETA |
| Lycopersicon esculentum | LPPWSISILPDCKNTVFNTARIGAQSAQMKMTSVSRG--LPPWSFNEETS |
| Cacao | LPPWSISILPDCKNTVFNTARIGAQSAQMKMTSVSRG--LPPWSFNEETS |
| Castor bean | LPPWSISILPDCKNTVFNTARIGAQSAQMKMTSVSRG--LPPWSFNEETS |
| Papaya | LPPWSISILPDCKNTVFNTARIGAQSAQMKMTSVSRG--LPPWSFNEETS *****:*****:***:*** * : ** .. :.***:***.* ** |
| | |
| Common tobacco | SYE-DSSFVTVVGLLEQINTTRDVS DYLVWYSTDVKIDSREGFLRSQKWPWL |
| Lycopersicon esculentum | SYE-DSSFVTVVGLLEQINTTRDVS DYLVWYSTDVKIDSREGFLRSQKWPWL |
| Cacao | SYE-DSSFVTVVGLLEQINTTRDVS DYLVWYSTDVKIDSREGFLRSQKWPWL |
| Castor bean | SYE-DSSFVTVVGLLEQINTTRDVS DYLVWYSTDVKIDSREGFLRSQKWPWL |
| Papaya | SYE-DSSFVTVVGLLEQINTTRDVS DYLVWYSTDVKIDSREGFLRSQKWPWL : : * ** :*****:***:*****:***:*** * ** : * * * TIMSAGHALHVFVNGQLAGTAYGSLEKPKLTFKAVNLRAGVNIISLSI TIMSAGHALHVFVNGQLAGTAYGSLEKPKLTFKAVNLRAGVNIISLSI TILSAGHALHVFVNGQLSGSAYGSLEFPKLTFSQGVNLRAGVNIISLSI TVLSAGHALHVFVNGQLSGTAYGSLESFKLTFKAVNLRAGVNIISLSI TVLSAGHALHVFVNDQLSGTAYGSLEFPKLTFSQGVNLRAGVNIISLSI *:*****.***:***** ** :***:***:***:***:***:***:***:*** |
| | |
| Common tobacco | AVGLPNIGPHFETWVAGVLPVSLGSLNEGKRDLTWQKWSYKVLKGEAL |
| Lycopersicon esculentum | AVGLPNIGPHFETWVAGVLPVSLGSLNEGKRDLTWQKWSYKVLKGEAL |
| Cacao | AVGLPNIGPHFETWVAGVLPVSLGSLNEGKRDLTWQKWSYKVLKGEAL |
| Castor bean | AVGLPNIGPHFETWVAGVLPVSLGSLNEGKRDLTWQKWSYKVLKGEAL |
| Papaya | AVGLPNIGPHFETWVAGVLPVSLGSLNEGKRDLTWQKWSYKVLKGEAL *****:*****:***:*** * : ** :***:***:***:***:***:***:***:*** |
| | |
| Common tobacco | SLHSLSGSSSVEWVEGSEFVAQRQPLTWYKTTFNAPAGNDPLALDLNMTMGK |
| Lycopersicon esculentum | SLHSLSGSSSVEWVEGSEFVAQRQPLTWYKTTFNAPAGNDPLALDLNMTMGK |
| Cacao | SLHSLSGSSSVEWVEGSEFVAQRQPLTWYKTTFNAPAGNDPLALDLNMTMGK |
| Castor bean | SLHSLSGSSSVEWVEGSEFVAQRQPLTWYKTTFNAPAGNDPLALDLNMTMGK |
| Papaya | SLHSLSGSSSVEWVEGSEFVAQRQPLTWYKTTFNAPAGNDPLALDLNMTMGK .*****. ***:***:*** * : ** :*****. ***** : *** |
| | |
| Common tobacco | GQVWINGQSIGRYWPGYKASGNCGACNYAGWFDEKKKCLSNCGEASQRWYH |
| Lycopersicon esculentum | GQVWINGQSIGRYWPGYKASGNCGACNYAGWFDEKKKCLSNCGEASQRWYH |
| Cacao | GQVWINGQSIGRYWPGYKASGNCGACNYAGWFDEKKKCLSNCGEASQRWYH |
| Castor bean | GQVWINGQSIGRYWPGYKASGNCGACNYAGWFDEKKKCLSNCGEASQRWYH |
| Papaya | GQVWINGQSIGRYWPGYKASGNCGACNYAGWFDEKKKCLSNCGEASQRWYH ** :***:***:***:***:***:*** * : ** :***:***:***:***:***:***:*** |
| | |
| Common tobacco | VPRSWLYPTGNLLVLFEEWGGEPHGISLVKREVASVCADINWQPQLVNW |
| Lycopersicon esculentum | VPRSWLYPTGNLLVLFEEWGGEPHGISLVKREVASVCADINWQPQLVNW |
| Cacao | VPRSWLYPTGNLLVLFEEWGGEPHGISLVKREVASVCADINWQPQLVNW |
| Castor bean | VPRSWLYPTGNLLVLFEEWGGEPHGISLVKREVASVCADINWQPQLVNW |
| Papaya | VPRSWLYPTGNLLVLFEEWGGEPHGISLVKREVASVCADINWQPQLVNW :**** .*****:*****:***:*****:***:*****:***:*****:***:***** |
| | |
| Common tobacco | MMQASGKVDKPLRPAKHLSCASGQKITSIKFASFGTPEGVCGSFREGSCH |
| Lycopersicon esculentum | MMQASGKVDKPLRPAKHLSCASGQKITSIKFASFGTPEGVCGSFREGSCH |
| Cacao | MMQASGKVDKPLRPAKHLSCASGQKITSIKFASFGTPEGVCGSFREGSCH |
| Castor bean | MMQASGKVDKPLRPAKHLSCASGQKITSIKFASFGTPEGVCGSFREGSCH |
| Papaya | MMQASGKVDKPLRPAKHLSCASGQKITSIKFASFGTPEGVCGSFREGSCH ** :***:***:***:*** * : ** :*****. ***** : ***:***:***:***:*** |
| | |
| Common tobacco | AFHSYDAFERYCIGQNSCSVPVTP-EIFGGDPCPHVMKLSVEVICS |
| Lycopersicon esculentum | AFHSYDAFERYCIGQNSCSVPVTP-EIFGGDPCPHVMKLSVEVICS |
| Cacao | AFHSYDAFERYCIGQNSCSVPVTP-EIFGGDPCPHVMKLSVEVICS |
| Castor bean | AFHSYDAFERYCIGQNSCSVPVTP-EIFGGDPCPHVMKLSVEVICS |
| Papaya | AFHSYDAFERYCIGQNSCSVPVTP-EIFGGDPCPHVMKLSVEVICS * .*****: * :*** ** :***.*** * : ** * .***:***:***:***:*** |

FIG. 2 THE ALIGNMENT OF THE PROTEINS ENCODED BY TOBACCO TBG1 GENE AND FOUR OTHER KINDS OF TBG1 PROTEINS

Results and Discussion

Isolation Result for Tobacco TBG1 Gene

For tobacco *TBG1* gene, through RT-PCR with pooled tissue cDNAs, the resulting PCR products were 2,526 bp (FIG. 1).

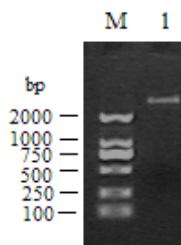


FIG. 1 PCR RESULT FOR TOBACCO *TBG1* GENE. M DL2000 DNA MARKERS; 1, PCR PRODUCT FOR TOBACCO *TBG1* GENE

Sequence Analysis

These cDNA nucleotide sequences analysis using the BLAST software at NCBI server (<http://www.ncbi.nlm.nih.gov/BLAST>) revealed that this gene was not homologous to any of the known tobacco gene and it was then deposited into the Genbank database (Accession number: KF267437).

The sequence prediction was carried out using the GenScan software and results showed that the 2,526-bp cDNA sequence represents one single gene which encodes 841 amino acids. The theoretical isoelectric point (pI) and molecular weight (Mw) of the deduced proteins of this tobacco gene were also computed using the Compute pI/Mw Tool (http://www.expasy.org/tools/pi_tool.html). The pI of tobacco *TBG1* is 6.68. The molecular weight of this putative protein is 93674.67.

Further BLAST analysis of these proteins revealed that tobacco *TBG1* has high homology with the *TBG1* of lycopersicon esculentum (Accession number: NP_001234303, 91%), cacao (Accession number: EOY27097, 81%), castor bean (Accession number: XP_002527409, 81%) and papaya (Accession number: ACP18875, 81%) (FIG. 2).

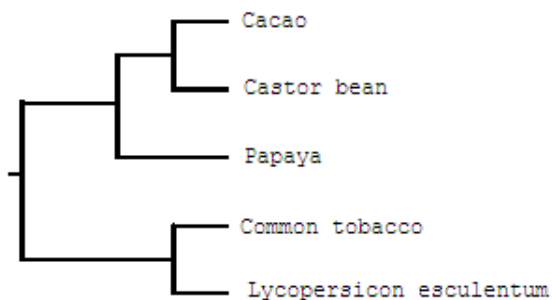


FIG. 3 THE PHYLOGENETIC TREE FOR FIVE KINDS OF *TBG1* GENES

Based on the results of the alignment of different species of *TBG1* proteins, a phylogenetic tree was constructed using the ClustalW software (<http://www.ebi.ac.uk/clustalw/>), as shown in FIG. 3. The phylogenetic tree analysis revealed that the tobacco *TBG1* gene has a closer genetic relationship with that of lycopersicon esculentum.

Tissue Expression Profile

Tissue expression profile analysis was carried out and results revealed that the tobacco *TBG1* gene was moderately expressed in flower and leaf, but hardly expressed in root and stem (FIG. 4).

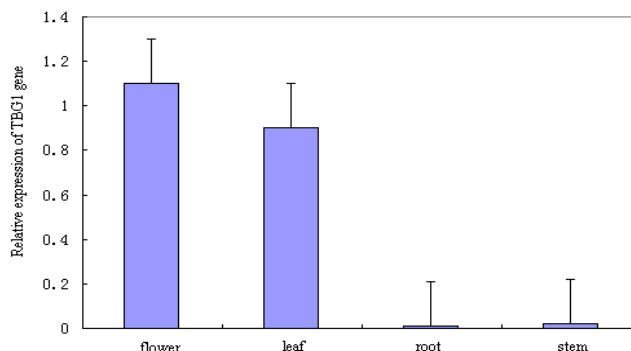


FIG. 4 EXPRESSION ANALYSIS OF *TBG1* GENE MRNA IN VARIOUS TISSUES

Comparative genomics research has revealed that virtually all (99%) of the protein-coding genes in humans align with homologs in mouse, and over 80% are clear 1:1 orthologs for human and mouse both belong to mammalian (Hardison, 2003). This extensive conservation in protein-coding regions implied that this conservation of protein-coding sequences may be expected in tobacco and lycopersicon esculentum as they are both plants of solanaceae. From sequence analysis of *TBG1* genes, it can be seen that the coding sequences of *TBG1* genes were highly conserved in some plants. This implied that the some plants can be utilized as model organisms and some tobacco genes can be isolated based on the coding sequence information of these plants.

The phylogenetic tree analysis revealed that the tobacco *TBG1* gene has a closer genetic relationship with that of lycopersicon esculentum. This implied that lycopersicon esculentum can be regarded as model organism to study the tobacco *TBG1* gene or tobacco can be utilized as model organism to study the lycopersicon esculentum *TBG1* gene.

From the tissue distribution analysis in our experiment, it can be seen that *TBG1* gene was obviously differentially expressed in some tissues. The suitable explanation for this under current conditions is that at

the same time those biological activities related to the mRNA expression of this gene were presented diversely in different tissues.

In conclusion, the tobacco *TBG1* gene was firstly isolated and then tissue expression profile analysis was performed; thus the primary foundation was established for further research on this tobacco gene.

REFERENCES

- Carey AT., Holt K., Picard S., Wilde R., Tucker GA., Bird CR., Schuch W., Seymour GB. "Tomato exo-(1-4)- β -d-galactanase: isolation, changes during ripening of normal and mutant tomato fruit and characterization of a related cDNA clone." *Plant Physiology* 108(1995):1099–1107
- Carey AT., Smith DL., Harrison E., Bird CR., Gross KC., Seymour GB., Tucker GA. "Down-regulation of a ripening-related beta-galactosidase gene (TBG1) in transgenic tomato fruits." *J Exp Bot.* 52(2001):663-668.
- Choi O., Lee Y., Han I., Kim H., Goo E., Kim J., Hwang I. "A simple and sensitive biosensor strain for detecting toxoflavin using β -galactosidase activity." *Biosens Bioelectron* 50C(2013): 256-261
- Fonseca-Berzal C., Merchán Arenas DR., Romero Bohórquez AR., Escario JA., Kouznetsov VV., Gómez-Barrio A. "Selective activity of 2,4-diaryl-1,2,3,4-tetrahydroquinolines on *Trypanosoma cruzi* epimastigotes and amastigotes expressing β -galactosidase." *Bioorg Med Chem Lett.* 23 (2013): 4851-4856
- Gross KC., and Sams CE. "Changes in cell wall neutral sugar composition during fruit ripening: a species survey." *Phytochemistry* 23(1984):2457–2461
- Hardison RC. "Comparative genomics." *PLoS Biol.* 1 (2003): E58.
- Li Y., Meng F., Yin J., Liu H., Si Z., Ni Z., Sun Q., Ren J., Niu H. "Isolation and comparative expression analysis of six MBD genes in wheat." *Biochim Biophys Acta* 1779 (2008):90–98
- Livak KJ., and Schmittgen TD. "Analysis of relative gene expression data using real-time quantitative PCR and the 2(-Delta Delta C(T)) Method." *Methods* 25(2001): 402-408.
- MS, Reid JSG. "Purification and properties of a novel β -galactosidase or exo-(1-4)- β -d-galactanase from the cotyledons of germinated *Lupinus angustifolius* L. seeds." *Planta* 192(1994): 502–511
- Shlush LI., and Selig S. "Digital Image Analysis of Cells Stained with the Senescence-Associated β -Galactosidase Assay." *Methods Mol Biol* 1048(2013):11-18.
- Smith DL., and Gross KC. "A family of at least seven β -galactosidase genes is expressed during tomato fruit development." *Plant Physiology* 123(2000):1173–1184
- Smith DL., Starrett DA., Gross KC. "A gene coding for tomato fruit β -galactosidase II is expressed during fruit ripening." *Plant Physiology* 117(1998):417–423

Characterization of Regolith Salt Storage in a Small Catchment of the Berg River Basin

Nebo Jovanovic^{*1}, Richard D.H. Bugar¹, Ashton Maherry¹, Louise Soltau¹, Willem P. De Clercq², Martin V. Fey²

¹Natural Resources and Environment, CSIR, PO Box 320, Stellenbosch 7599, South Africa

²Department of Soil Science, University of Stellenbosch, Private Bag X1, Matieland 7602, South Africa

*njovanovic@csir.co.za

Abstract

Dryland salinity recharge from agricultural land has been identified as the main source of salinization in the Berg river basin (Western Cape, South Africa), which represents a challenge to water users and water quality managers. The aim of this study was to characterize and quantify regolith salt storage in a small catchment (~ 20 ha) representative of the saline environment and drier bio-climatic conditions of the mid- and lower reaches of the Berg river basin, where storage and potential discharge of salts are likely to be the greatest. Electromagnetic induction measurements with an EM-38 meter indicated that salinity in the landscape is driven by the topo-sequence, anti-erosion contours act as barriers to water and salt fluxes, highly saline scalds are associated with convex hillslopes, and soil salinity is lower at the end of the rainy winter season compared to that at the dry summer. Resistivity tomography measurements taken with an ABEM Terrameter SAS1000 ground imaging apparatus down to approximately 70 m depth indicated that subsurface drainage features are often associated with salinity and topographic flow pathways, as a result of shale weathering. Analyses of core samples collected during borehole drilling indicated that the regolith contains about 400 tons of salts per hectare, stored mainly as a bulge in the unsaturated vadose zone (between about 5 and 10 m depth), above the water table and below the soil zone, discharging mainly through lateral leaching by groundwater from the phreatic zone. Groundwater quality becomes increasingly saline from the recharge area (0.68 dS m⁻¹) towards the bottom end of the catchment (3.75 dS m⁻¹), and it is a mixed cation-chloride-type. The effects of different climates, hydrogeological characteristics and land uses on the salt discharge into the mid- and lower reaches of the Berg river need to be investigated.

Keywords

Dryland Salinity; Electromagnetic Induction; Groundwater Quality; Regolith; Resistivity Tomography

Introduction

Salinization of soil and water resources is usually associated with irrigated agriculture (Van Rensburg, De Clercq, Barnard and Du Preez, 2011). However, the

occurrence of dryland salinity is widespread throughout semi-arid regions of the world, with associated impacts on water resources, ecosystems and land productivity (Pannell, McFarlane and Ferdowsian, 2001; Clarke, George, Bell and Hatton, 2002). The process of dryland salinization occurs either through weathering of rock minerals or salts may be brought into the landscape from the ocean, by rain or wind (Hingston and Gailitis, 1976; Acworth and Jankowski, 2001). Studies conducted in Australia have produced evidence that dryland salinity may be exacerbated by human activities (Greiner, 1998; Stirzaker, Cook and Knight, 1999; Angus, Gault, Peoples, Stapper and Van Herwaarden, 2001; Clarke, George, Bell and Hatton, 2002). In particular, clearing of natural perennial scrubland to make way for cultivated crops and pastures has resulted in changes in the water balance, rising groundwater tables and mobilization of fossil connate salts (Pannell and Ewing, 2006).

In South Africa, dryland salinity is common in the Berg river catchment (Western Cape Province). The South African Department of Water Affairs (formerly Department of Water Affairs and Forestry) has monitored Berg river salinization since the mid 1970's. A cycle of research projects funded by the Water Research Commission (Fey and De Clercq, 2004; Gorgens and De Clercq, 2005; De Clercq, Jovanovic and Fey, 2010) indicated that irrigated agriculture does not account for the Berg river salinization, rather salinity recharge from dryland agriculture is the main source of salinity. This is an enormous challenge because of the variety of water users (drinking water supply, agricultural, industrial, ecosystems, recreational), each requiring specific volumes and qualities of water (DWAF, 2004). Characterization and quantification of natural salts in the regolith is therefore important in order to determine the extent and hazard of salinization, to identify saline scalds as major contributors to runoff salinity (Hughes, Khan, Crosbie,

Helliwell and Michalk, 2007), as well as to model and predict salinity processes.

Estimates of salt accretion and storage in the unsaturated regolith and groundwater in Western Australia were made by Johnson (1987) and McArthur, Churchward and Hick (1977), whilst Engel, McFarlane and Street (1989) used geophysics and drilling to characterize flow pathways (in Clarke, George, Bell and Hatton, 2002). Acworth and Jankowski (2001) carried out perhaps the most comprehensive study on the source of salts causing dryland salinity in a small catchment in New South Wales (Australia) by using drilling, geophysics, hydrogeochemistry and groundwater monitoring. Acworth (1999) used electromagnetic ground conductivity meters to obtain 2-dimensional vertical sections of salinity-induced apparent electrical conductivities. These data could then be correlated to electrical conductivity (EC) values obtained from soil solution and borehole drilling core extracts, groundwater quality and other field data. Bennett and George (1995) measured soil salinity with an electromagnetic induction meter in order to determine the salinity effects on growth of Eucalyptus plantations planted to lower groundwater tables in South-Western Australia. Stirzaker, Cook and Knight (1999) supplied analytical expressions to determine salt accumulation in the root zone from shallow water tables under different agroforestry systems. Other Australian studies were focused on relating the increase in water table level to the extent of land salinization. For example, Greiner (1998) used a spatial optimization model for analyzing catchment management (SMAC) to predict salinization as affected by current land use, optimized land use scenario, and including climatic variability. Clarke, George, Bell and Hatton (2002) discussed extensively how the geology and land use changes in South-Western Australia affect water flow pathways and recharge.

In the Berg river catchment, salt storage was seldom measured. The only comprehensive study done so far was that of Flugel (1995), who used drilling, soil mapping as well as measurements of soil water and groundwater salinity to quantify the storage of salts at several locations and estimated the salt balance in the Sandspruit catchment. Sandspruit is a tributary of the Berg river approximately 150 km² in size, located in quaternary catchment G10J as delineated by the Department of Water Affairs. The aim of the current study was to characterize and quantify the salts stored in the regolith of a small catchment representative of the saline environment in the Berg river basin. The

small catchment is located in quaternary catchment G10F, adjacent to and with a similar hydrogeological set-up as Sandspruit.

Site Description

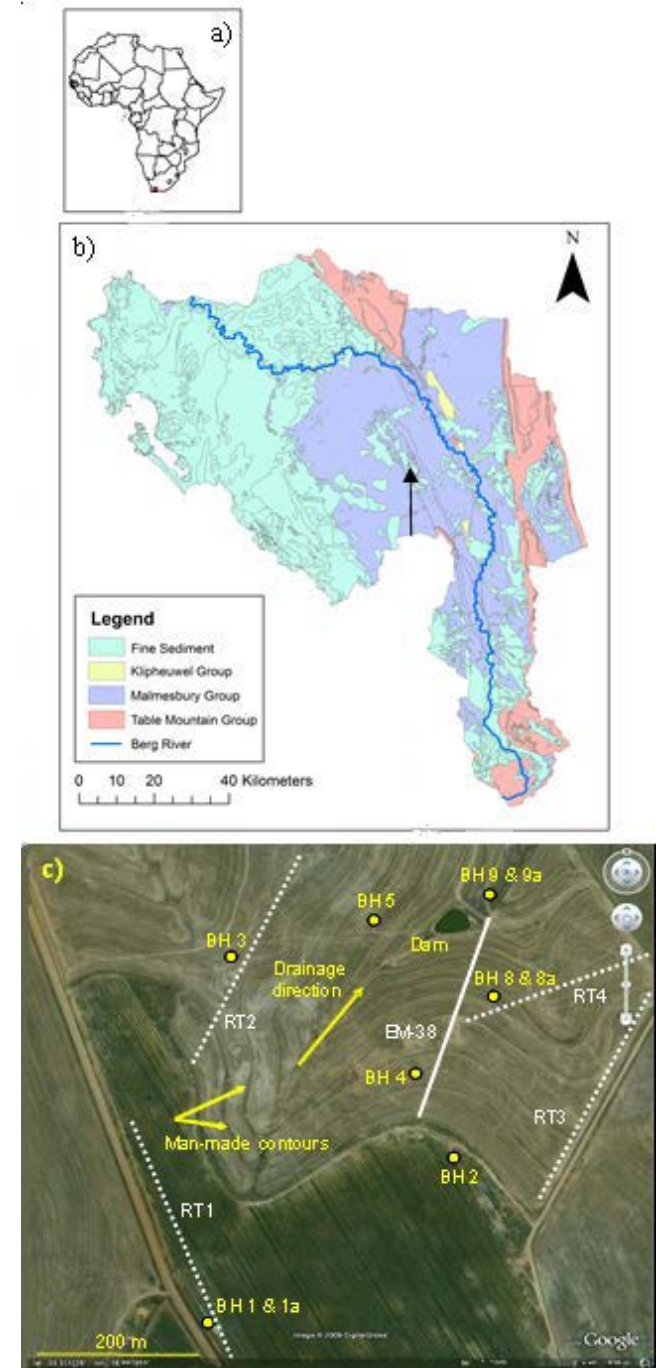


FIG. 1 (a) LOCATION OF THE STUDY AREA IN AFRICA, (b) GEOLOGICAL MAP OF THE BERG RIVER BASIN (1:250,000, AVAILABLE AT <http://www.geoscience.org.za>, ACCESSED 26 MARCH 2009) AND (c) LOCATION OF THE GOEDERTROU SMALL CATCHMENT IN Google Earth. THE POSITIONS OF BOREHOLES (BH), RESISTIVITY MEASUREMENT TRANSECTS (DASHED LINES RT), ELECTROMAGNETIC INDUCTION MEASUREMENT TRANSECT (SOLID LINE EM-38), STOCK-WATERING DAM AND MAN-MADE CONTOURS ARE INDICATED

The source of the Berg river is in the Franschoek and Jonkershoek mountains (East of Cape Town) and it flows in a north-westerly direction where it eventually discharges into the sea at Velddrif (Fig. 1b). The Berg river is approximately 270 km in length and has a catchment size of about 900 km² (DWAF, 1993). A large part of the catchment is located in semi-arid wheat lands which receive most of their rain during the winter months (450 mm a⁻¹ on average, mainly from May to October). The geology of the Berg river basin is dominated by the Malmesbury Group shales (western banks, grey shade in Fig. 1b) and the Table Mountain Group sandstones (eastern banks, light brown shade in Fig. 1b).

The Malmesbury Group is a proterozoic marine deposit comprising greywacke and phyllite beds, with beds and lenses of quartz schist, limestone and grit. The Malmesbury Group Aquifer occurring in the area is classified as a Minor Aquifer System (Parsons, 1995). This is defined as fractured or potentially fractured rocks that do not have a high primary permeability, or other formations of variable permeability. Their extent may be limited and water quality variable. Although these aquifers seldom produce large quantities of water, they are important for both local supplies and discharge as baseflow into rivers. They also have a moderate vulnerability to pollution. Regional groundwater flow is towards the Berg river, and thereafter, parallel to the river in the western part of the catchment (Fig. 1b).

In order to characterize and quantify the regolith salt storage in the typically saline environment, a small catchment located on the Goedertrou farm was selected, 5 km North-East of the town of Riebeek West and approximately 70 km North of Cape Town in the Western Cape Province. The Google Earth view of the Goedertrou catchment is shown in Fig. 1c (latitude 33°18'33.16" S; longitude 18°53'40.67" E; altitude 120 m at a stock-watering dam collecting runoff and interflow water). The Goedertrou catchment is ~20 ha in size and deemed to be representative of the area in terms of soils (residual soils with differing sand, clay and gravel contents generally overlie silcrete and weathered Malmesbury Group shales), topography (slope ~10% on average), land use (dryland winter wheat cropping followed by two years of fallow grazing; and vineyard) and land management (man-made anti-erosion contours; shallow tillage to break up the soil surface crust). In addition, the site is representative of the drier bio-climatic conditions in the mid- and lower reaches of the Berg river, where

storage and potential discharge of salts are likely to be the greatest. The Goedertrou catchment receives less than the average rainfall for the Berg river catchment due to topographic conditions (approximately 330 mm a⁻¹) with an average annual potential evaporation of 1615 mm. The general slope is from the South-West to the North-East with the main surface drainage features described by the man-made anti-erosion contours visible in Fig. 1c.

Pedological, chemical and physical characteristics of the soils were characterized in approximately 1.2 m deep pits, excavated on a 50x50 m grid. The dominant soil forms are Glenrosa (Soil Classification Working Group, 1991)-Cambisol (FAO, 1998) and Swartland (Soil Classification Working Group, 1991) - Luvisol (FAO, 1998). The detailed pedological, chemical and physical information on the soils at Goedertrou were reported by De Clercq, Jovanovic and Fey (2010).

Material and Methods

The approach used to characterize salinity and salt storage in the Goedertrou small catchment included electromagnetic induction measurements, geophysics and borehole establishment.

Electromagnetic Induction

Electromagnetic induction is a non-invasive technique that measures electrical conductivity by inducing an electrical field in the soil. Apparent electrical conductivity of the bulk soil is measured and this represents a combination of soluble salts, clay content and mineralogy, porosity, structure, bulk density, cation exchange capacity, soil water content and temperature (McNeill, 1980; Corwin and Plant, 2005).

The EM-38 electromagnetic induction meter (Geonics Ltd., Mississauga, Ontario, Canada) was used to map soil salinity in the Goedertrou catchment. The measurements were taken during April 2005, on a 1 m x1 m grid. The meter was positioned vertically in order to scan a soil depth of between 0.15 m and 1.5 m. A transect on the North-facing slope of the catchment was then scanned in October 2006 (end of rainy winter season) and April 2007 (end of dry summer season) at approximately 10 cm intervals. The meter was positioned vertically and horizontally in order to scan two soil depths, namely 0.15-1.5 m (vertical reading) and 0.3 m (horizontal reading). The location of the transect is shown in Fig. 1c. The purpose of the transect measurements was to assess the seasonal change in bulk soil salinity, as well as the link between salt distribution in the landscape, salinity profile and

topography.

Resistivity Tomography

Resistivity tomography is a non-invasive technique that was used to provide a pseudo-section of change in electrical properties in the subsurface along a specified line (transect). The bulk resistivity of porous rocks varies mostly because of changes in porosity and saturation of the host rock and salinity of the pore fluid (Telford, Geldart, and Sheriff, 1990), in the absence of clay. In the presence of clay (from weathering of the Malmesbury shale in this case), a surface conduction term has to be included (Bussian, 1983). Relatively, the high clay content and high salinity of the pore fluid will result in a very low resistivity for the subsurface.

The resistivity measurements were taken with an ABEM Terrameter SAS1000 ground imaging apparatus. The measurement sequence is controlled by the ABEM electrode selector ES464 (ABEM Instrument AB, Sweden). Two multi-core cables with 21 electrode take-outs every 10 m were used. The cables were laid out on the ground, consecutively from start to end, in a straight line to cover a transect of 400 m. An electrode (metal stake) was inserted into the ground next to every electrode take-out on the cable. The electrode take-out was then connected to the electrode with a short cable jumper. The data were collected using a standard protocol of the Schlumberger-Wenner array (Loke, 2001). All data were acquired for $a = 1$ to 8 and $n = 1, 2$ and 4, where 'a' is the electrode separation multiplication factor and 'n' is the electrode spacing multiplication factor. The apparent resistivity data acquired in the field were inverted using the RES2DINV software (Loke, 2001) to provide a pseudo-section of changes in resistivity along each profile.

Resistivity measurements were taken during September 2005, along the transects shown in Fig. 1c. The depth of investigation for this particular set-up was about 70 m. The resistivity method was applied to define subsurface drainage. The envisaged drainage pattern would be reflected in deeper channels of weathering in the underlying shale which is related to fracture zones. It was expected that surface drainage in the small catchment is partly controlled by geological characteristics. The transect locations were selected in such a way to cross expected drainage patterns perpendicularly, as well as to minimize the effects of increased wetness (caused by damming of anti-erosion contours) on the resistivity readings. The resistivity measurements in transects generally

parallel to topographic contours were therefore used to identify geologically-driven drainage patterns.

Borehole Drilling and Sampling

Following the results obtained from resistivity and the identification of geologically-driven drainage patterns, nine boreholes were installed in the Goedertrou catchment from March to April 2005 in order to obtain background information on the aquifers. The boreholes were drilled using a rotary percussion rig. Undisturbed and disturbed unsaturated zone samples were taken during drilling down to the water table or to a maximum depth of 25 m. The samples were taken at either 0.5 m (tube method) or 1 m (auger-tip method) interval depths. Fifty tube and 80 auger-tip samples were taken in total. All samples were sealed immediately after being taken in order to prevent contamination and evaporation. A full set of laboratory chemical analyses was done on the saturated paste extracts of these regolith core samples. Borehole information was logged for all boreholes.

Borehole casing was 125 mm diameter Class 12 PVC (with stabilisers) to termination depth, with screened sections placed adjacent to water strikes. Sand was used as stabilization material adjacent to screened intervals, whilst gravel was positioned on solid sections. Bentonite seals were also installed where appropriate in order to prevent shallow groundwater from entering into boreholes as well as the ingress of surface runoff. Groundwater was sampled after borehole installation was completed. As part of this process, boreholes were purged with a submersible pump at a rate of 0.75 L s^{-1} for a predetermined amount of time, equal to three times the borehole casing volume. The groundwater samples were then taken, placed immediately into a cooler box in the field and transferred to a refrigerator in the laboratory on the same day of sampling. A full set of laboratory chemical analyses was done on the groundwater samples.

Results

Electromagnetic Induction

A soil salinity map for the Goedertrou catchment was developed using measurements taken with the EM-38 meter in April 2005 (Fig. 2). The data collected on a 1 m x 1 m grid represented the vertical scan (0.15-1.5 m depth), and these were interpolated using ordinary kriging. The map shows that bulk soil salinity varied between approximately 20 and 160 mS m^{-1} across the

small catchment (Fig. 2). The Goedertrou catchment has a soil mantle that is variably saline and this is possibly attributable to salt influx from an extensive recharge zone at the top of the catchment or to exposure of saline saprolite through natural erosion. The poorly structured, low carbon topsoil (with a clay fraction consisting chiefly of kaolinite and mica), although lighter textured than the subsoil, exhibits strong crusting. Runoff during rain events is consequently intense (De Clercq, Jovanovic and Fey, 2010). The more clayey subsoil, low hydraulic conductivity and high compaction (average bulk density in the B-horizon, where present, is 1.89 g cm^{-3}) represents a further barrier to groundwater recharge, and lateral migration of perched water through the surface horizon is therefore common.

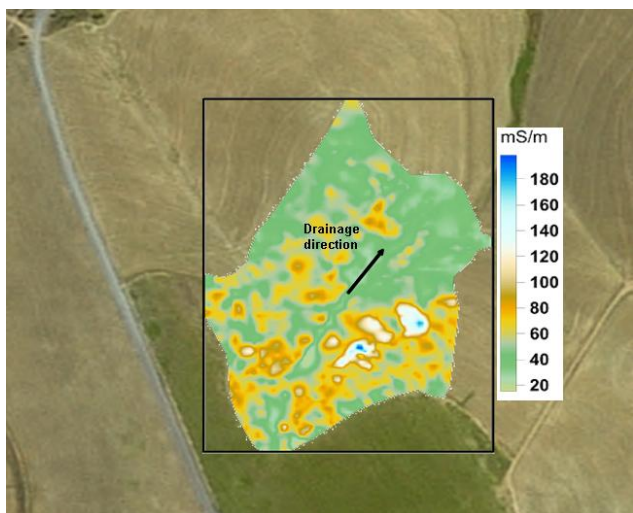


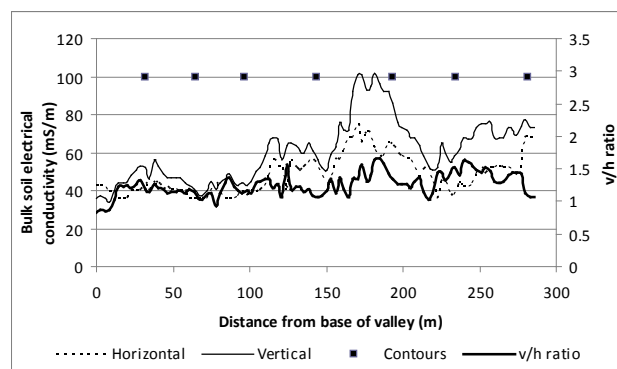
FIG. 2 EM-38 SCAN OF THE GOEDERTROU CATCHMENT INDICATING SALINITY (mS m^{-1}) AND THE SPATIAL DISTRIBUTION THEREOF IN THE CATCHMENT (AFTER DE CLERCQ, JOVANOVIC AND FEY, 2010)

Bulk soil salinity was generally higher on the North-facing slope, in particular at a convex position on the mid-slope, where salinity effects were visible in the form of a saline scald where wheat failed to germinate. In most of these very saline spots, the B horizon is absent leaving a very thin A horizon directly on shale. Down-slope leaching from the crest and down-valley leaching from the foot-slope soils could possibly account for this mid-slope salinity maximum.

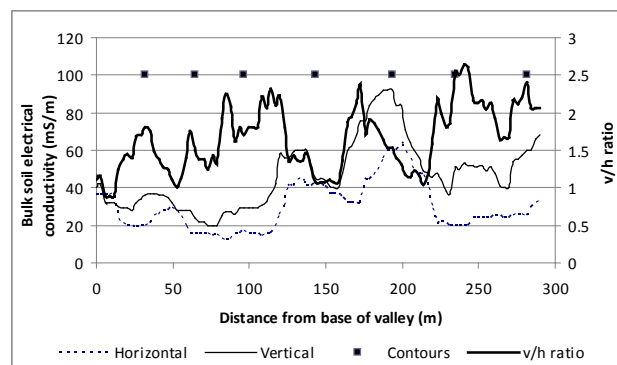
The vertical and horizontal scans obtained with the EM-38 meter on the North-facing hillslope transect (Fig. 1c) are shown in Fig. 3. The measurements were taken in late winter (October 2006) when most salts were washed away and/or back into the soil through infiltration, and at the end of summer (April 2007) when the soils were driest and a lot of salt occurred on and/or close to the soil surface. The EM-38 data

represent the average bulk soil EC at each measuring point over the measuring depth. The square blocks in Fig. 3 indicate the position of the contour banks.

In general, bulk soil salinity values were lower in October 2006 compared to April 2007. The saline scald identified in the salinity map (Fig. 2) is also recognizable in the mid-slope area of the transect (Fig. 3; 150-200 m distance from base of valley). It is also clear that salinity in the landscape varies at different sections of the topo-sequence and that anti-erosion contours have a marked effect on salinity distribution in the catchment.



(a)



(b)

FIG. 3 BULK SOIL ELECTRICAL CONDUCTIVITY VERTICAL AND HORIZONTAL READINGS TAKEN WITH AN EM-38 METER ON A NORTH-FACING HILLSLOPE TRANSECT BEFORE (APRIL 2007 (a)) AND AFTER WINTER RAINS (OCTOBER 2006 (b)), AND SMOOTHED RATIOS OF VERTICAL AND HORIZONTAL (v/h) READINGS (MOVING POINT AVERAGE OF NINE READINGS) (AFTER CLERCQ, JOVANOVIC AND FEY, 2010)

The smoothed ratio of vertical and horizontal readings (moving point average of nine readings) were also compared for October 2006 and April 2007 in order to investigate differences in soil salinity profiles along the hillslope transect (Fig. 3). The ratio declined and approached 1 towards the base of the valley meaning that, lower down in the catchment, a homogeneous profile of salt seemed to be the norm. In the upper part of the catchment, the vertical reading was much higher than the horizontal reading, indicating much

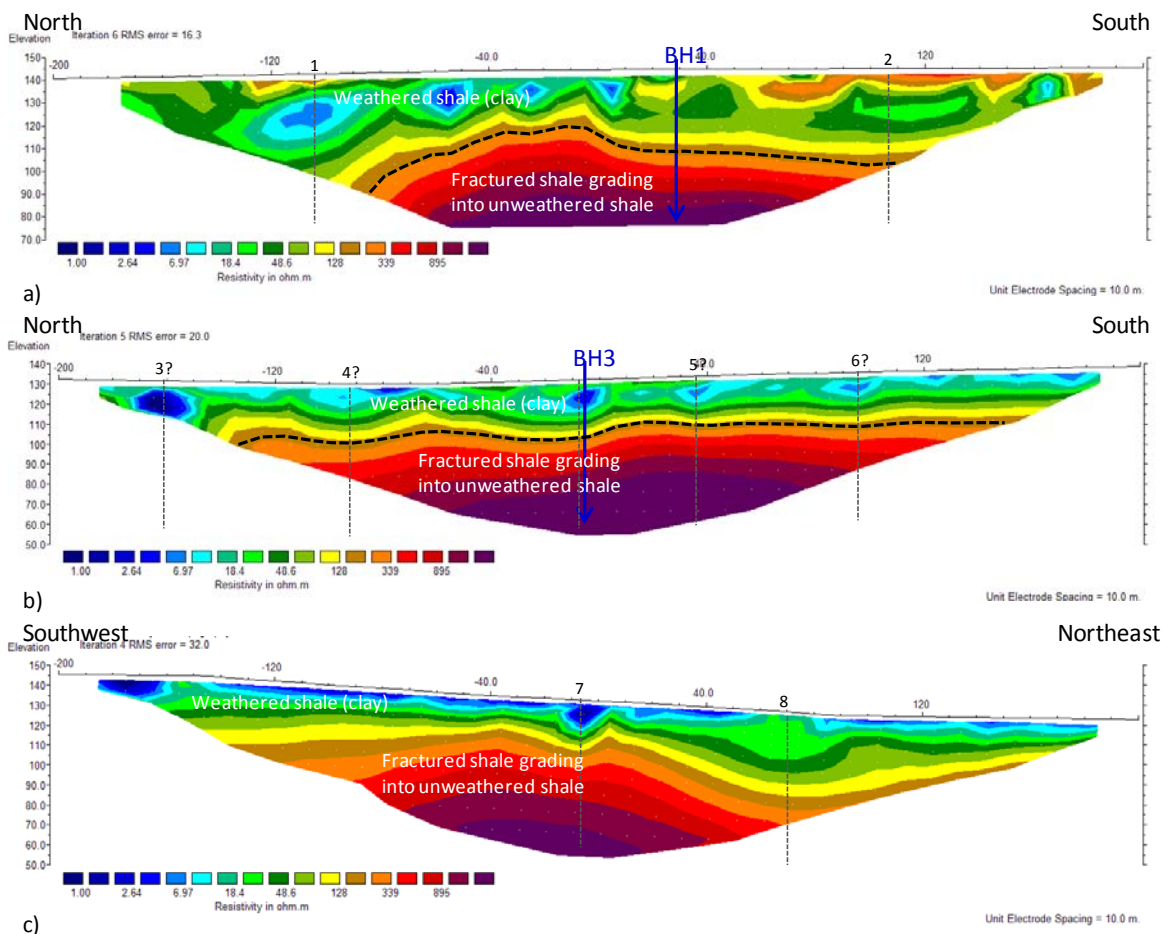
more salts lower down in the soil profile compared to the soil surface layer.

Resistivity Tomography

The inverted resistivity profiles for transects RT1 to RT4 (Fig. 1c) are shown in Fig. 4. The resistivity scale along all profiles has been normalised to aid comparisons. The distance and depth along all profiles are approximately the same. In general, all the profiles show a shallow very low to low resistivity layer (1 to ~250 ohm.m) that corresponds to the weathered Malmesbury Shale (clay). This is underlain by a higher resistivity layer (> 250 ohm.m) corresponding to the fractured shale that grades into unweathered shale at greater depths. This correlates well with previously established resistivity values for shale; and from previous resistivity studies in shale, it has been established that the fractured shale has a resistivity of between 200 and 500 ohm.m (Soltau and Anderson, 2006). The resistivity for unweathered shale is often above 500 ohm.m, but usually does not exceed 2000 ohm.m (Soltau and Anderson, 2006).

For transect RT1 (Fig. 4a), the resistivity cross-section shows a low resistivity top layer that corresponds to the weathered shale. The interface between the clay

(weathered shale) and fractured shale has been interpolated from the borehole log information for BH 1. The northern half of the profile shows a lower resistivity at intermediate depth which is likely to correspond to high salinity pore fluid. Along this profile, there are 2 likely subsurface fracture zones (features 1 and 2) related to subsurface drainage. It is not clear whether these correspond to surface drainage in any way. The underlying higher resistivity layer corresponds to the fractured shale that grades into unweathered shale. The resistivity cross-section also shows two high resistivity sections along the shallow part of the profile. This does not occur on any of the other profiles. The northern part of the profile is started in a silcrete lens that is part of the paleo-weathering African Surface. This accounts for the high resistivity at shallow depth, however the change in resistivity towards the end of the profile is not very clear. This could be an indication of transported silicate material, which has a much higher resistivity than the clay material. It could also in itself indicate a paleo-weathering surface, as it is fairly level and homogenous. It does, however, also show deeper weathering that could be related to multiple fracture zones (feature 2 in Fig. 4a).



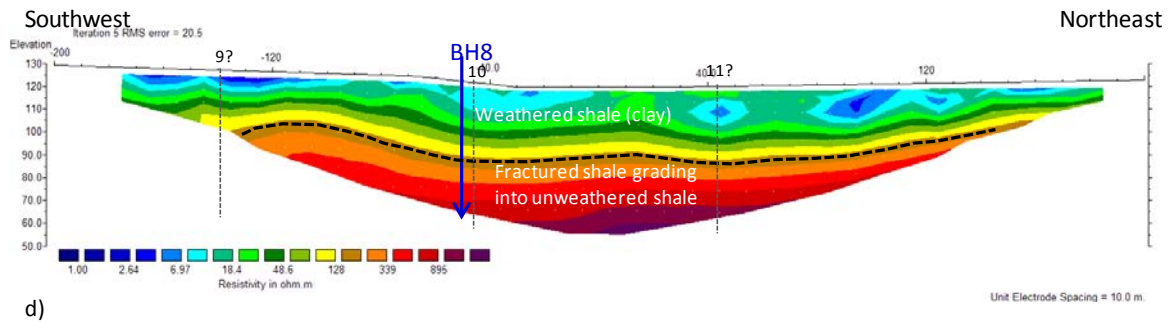


FIG. 4 INVERTED RESISTIVITY DATA FOR TRANSECTS RT1 (a), RT2 (b), RT3 (c) AND RT4 (d) WITH BOREHOLE POSITIONS (BLUE ARROWS) AND INTERPRETED FRACTURE FEATURES (GRAY DOTTED LINES)

The resistivity cross-section for transect RT2 (Fig. 4b) shows a shallow subsurface layer with low to very low resistivity that corresponds to the weathered shale. The very low resistivity that occurs in the shallow subsurface, towards the northern end of the profile, is indicative of high salinity, clay soils. The very low resistivity zones along this profile correspond to zones of fracturing/preferential weathering, but this is a lot less pronounced compared to transect RT1. Undulations along the weathered surface on this profile are less pronounced. The general depth of weathering is also not as deep as that in the previous profile of RT1. A number of potential fracture features have been delineated, but it was also not clear whether these correspond to surface drainage. BH 3 coincides with the most obvious fracture feature along this profile and seems to coincide with a shallow surface drainage channel.

The inverted resistivity profile for transect RT3 (Fig. 4c) shows the shallow subsurface layer with low to very low resistivity (clay) and the deeper higher resistivity layer (fractured shale). There is no borehole information to verify the interpretation along the profile. Similar to RT2, the depth of weathering seems to be shallower. Also, the very low shallow resistivity zone occurs across most of the profile and the saline soil is more evenly developed along this profile. Two potential fracture features have been indicated on the profile (Fig. 4c). Feature 7 coincides with a surface drainage feature and this is likely controlled by the subsurface fracturing.

The resistivity cross-section for transect RT4 (Fig. 4d) shows the shallow subsurface layer with low to very low resistivity (clay) and the deeper higher resistivity layer (fractured shale). The low resistivity values along the southwestern part of the profile coincide with the saline scald that has been identified in the field and verified on the shallow electromagnetic survey. Two potential fracture features were delineated (9 and 11 in Fig. 4d; it is not clear if they correspond to surface

drainage). Feature 10 near borehole 8 coincides with a surface drainage pathway.

Borehole Drilling and Sampling

The geology of the catchment consists of a surficial drape of colluvial/alluvial material overlying rocks of the Moorreesburg Formation, which forms part of the Namibian Malmesbury Group. The shales themselves typically vary from highly-to-slightly weathered in character, with the effects of weathering becoming less pronounced with depth. The weathering characteristics of the material vary from highly leached kaolinitic clay underlying the eroded silcrete of the African Surface, to mottled clay in the lower banks of the catchment. Unconsolidated alluvium overlies this weathered material in the drainage feature that bisects the catchment, its depth increasing towards North-East. Two aquifers occur within the study area itself; a shallower, perched aquifer restricted to the weathered zone of the Moorreesburg Formation, and a deeper aquifer in the relatively unweathered shale. Four boreholes were drilled to depths between 20 and 30m, namely 1a, 5, 8a and 9a (Fig. 1c), the remaining five to depths between 40 and 80m. Borehole 2 was already established on the farm.

The regolith salinity profiles for five boreholes are shown in Fig. 5. The data represent values of electrical conductivity measured on saturated paste extracts (EC_e) of material collected at 1 m depth increments during drilling. Although boreholes 8 and 9 have incomplete salinity profiles (Fig. 5), they are not inconsistent with the full pattern shown for boreholes 3, 4 and 5. This pattern can be summarised as reflecting a progressive increase in salinity from low to moderate values at the surface to a peak value at a depth of between 5 and 10 m. Thereafter, salinity decreases asymptotically to a stable EC_e value of less than 1 dS m^{-1} . It was hypothesised that this decrease results from the lateral leaching of accumulated salts by moving groundwater. Accordingly, salt storage

within the regolith is revealed as occurring predominantly within the vadose zone, but beneath the soil zone (from which it is leached downward by infiltrating rainwater) and above the saturated zone as commonly defined hydrologically.

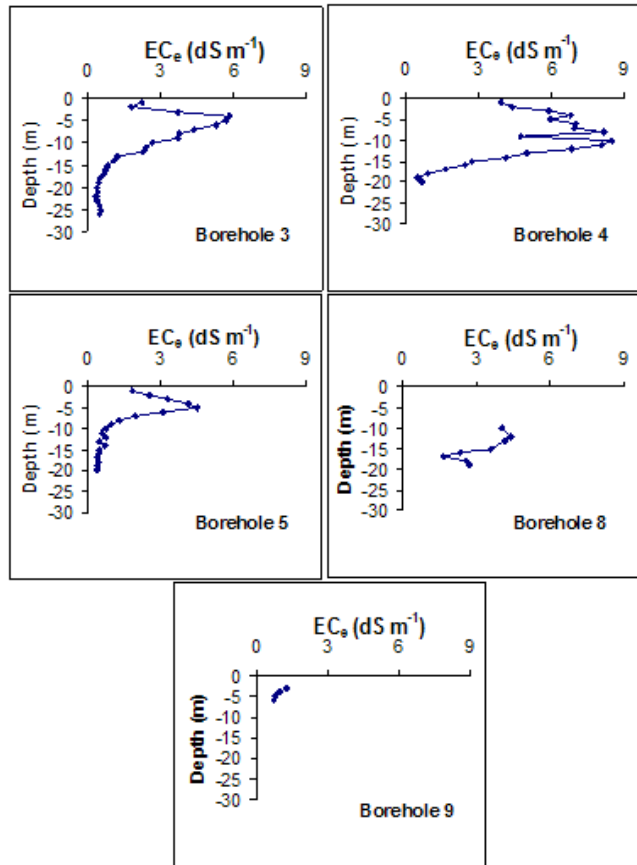


FIG. 5 REGOLITH SALINITY PROFILES FROM SATURATED PASTE EXTRACTS (EC_e) OF SAMPLES OBTAINED AT 1 m DEPTH INCREMENTS FROM FIVE BOREHOLES DRILLED IN THE GOEDERTROU CATCHMENT

Thus, for borehole 5, the salinity peak at about 5 m depth is illustrated in Fig. 6 due to the combined reduction in relative frequency with which the downward moving wetting front and upward migrating water table enter the zone of maximum salt accumulation. The shape and magnitude of the salinity bulge will likely depend also on the extent to which upward and downward dissolution fronts overlap, as well as the rate at, and extent to which both perched- and groundwater discharge laterally.

For reference purposes, an EC_e value of 1 dS m^{-1} represents a soluble salt content of about $6 \text{ t ha}^{-1} \text{ m}^{-1}$. This has important implications for estimating salt storage in whole catchments. From the data for boreholes 3, 4 and 5 (Fig. 5), the regolith was calculated to contain 333, 608 and 186 t ha^{-1} of soluble salts for the three boreholes respectively, the bulk of

which is in the vadose zone. A mean value of about 376 t ha^{-1} is therefore suggested for the small catchment. In comparative terms, Brouwer and van de Graaff (1988) estimated 500 t ha^{-1} are stored in weathered regolith (pallid zone) at Gatun in Western Victoria (Australia) (in Brouwer and Fitzpatrick, 2002a and b).

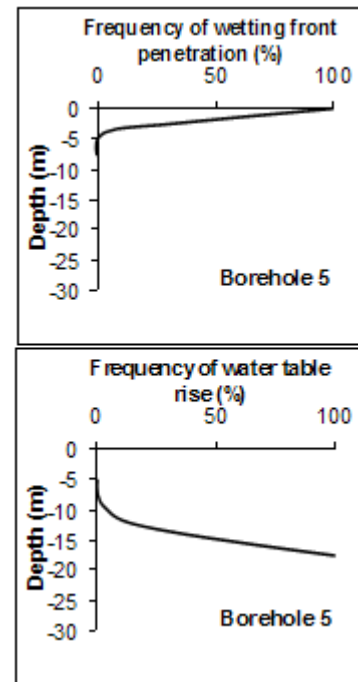


FIG. 6 HYPOTHETICAL WETTING EFFECTS OF RAINWATER AND GROUNDWATER ON THE PRODUCTION OF THE SALT BULGE IN THE REGOLITH AT BOREHOLE 5, GODETROU CATCHMENT



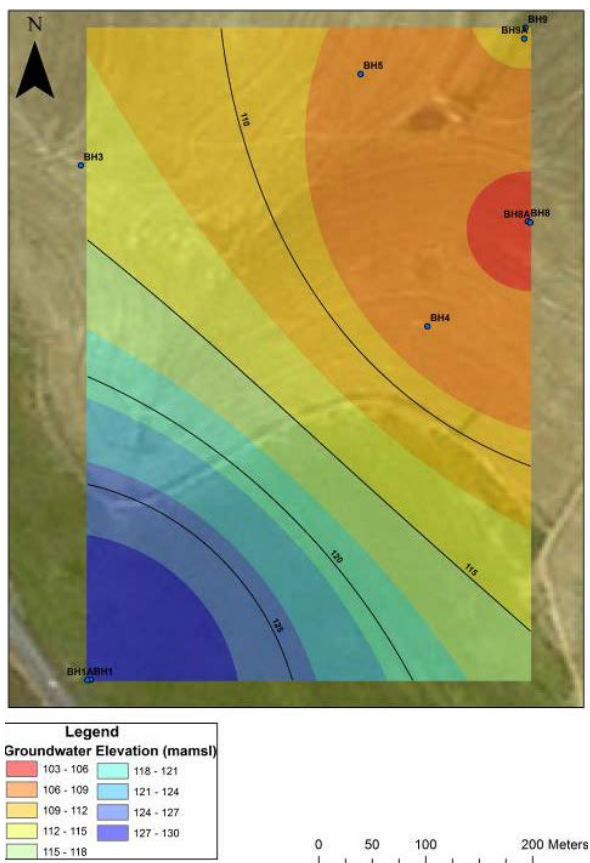


FIG. 7 TOPOGRAPHIC CONTOURS (mamsl, TOP) AND GROUNDWATER ELEVATION INTERPOLATED FROM MEASUREMENTS IN THE BOREHOLES (RIGHT) IN THE GOEDERTROU CATCHMENT

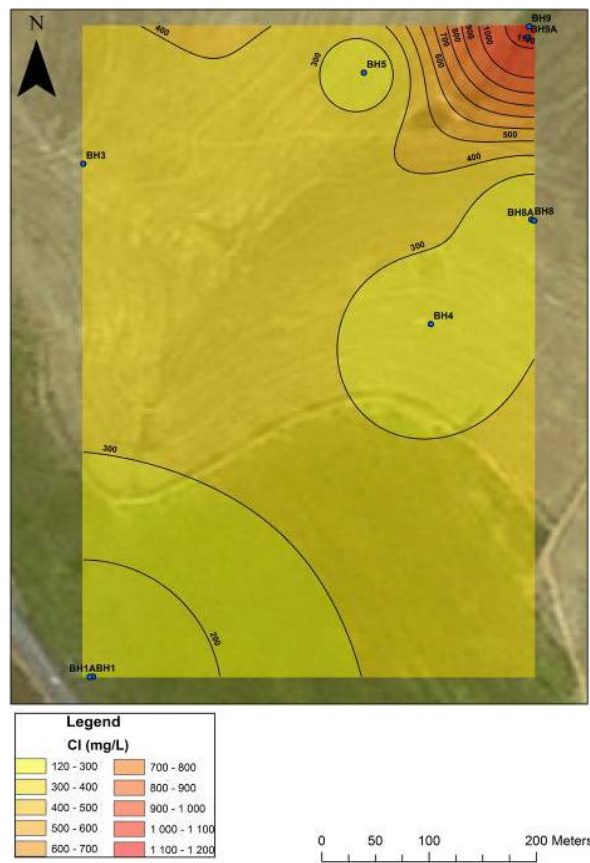
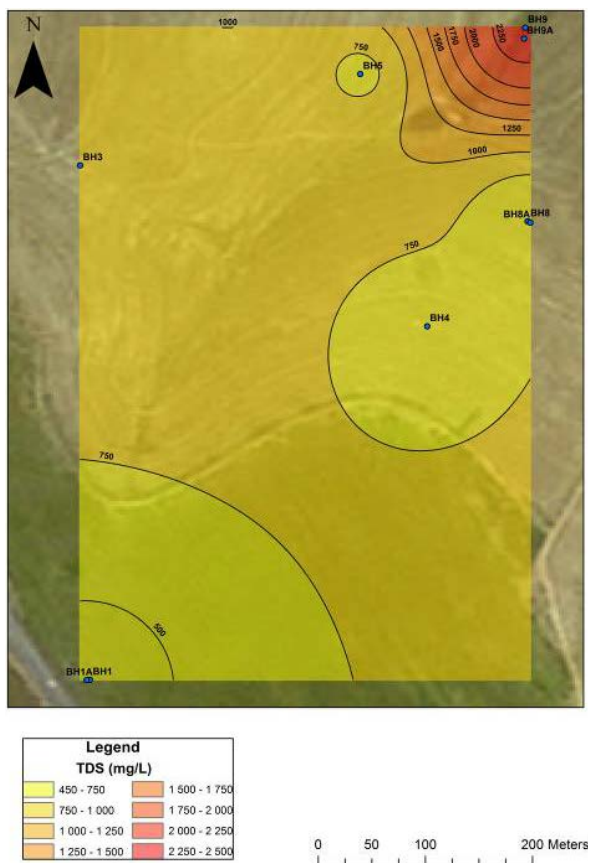


FIG. 8 TOTAL DISSOLVED SALTS (TOP) AND CHLORIDE CONCENTRATION (BOTTOM) INTERPOLATED FROM WATER QUALITY MEASUREMENTS IN THE BOREHOLES IN THE GOEDERTROU CATCHMENT



The rest water level and the groundwater quality were measured in the new boreholes. The interpolated groundwater level surface indicates groundwater flow from the South-West to the North-East (Fig. 7). There was a good correlation between water levels and topography with a $R^2 = 0.89$, implying that the aquifers are semi-confined. The interpolated data map of the groundwater total dissolved salts (TDS) distribution shows a general increase in TDS with decrease in water level elevation (Fig. 8). A similar trend of increase in chloride concentration with decrease in water level elevation was also observed (Fig. 8).

Significantly, groundwater quality became increasingly saline towards the bottom end of the catchment (Fig. 8). Based on chemical analyses, EC in the groundwater varied between 0.68 (borehole 1) to 3.75 dS m^{-1} (borehole 9). In borehole 3, EC was 1.26 dS m^{-1} , which, in terms of the volumetric salt content it represents, is roughly consistent with EC_c values of about 0.5 dS m^{-1} in disturbed auger samples below a depth of about 15 m (Fig. 5).

Site groundwater is perhaps best classified as being of mixed cation-chloride-type, and appears to have

similar characteristics across the study area (Fig. 9). The piper diagram in Fig. 9 indicates that Na^+ and Mg^{2+} dominate amongst cations, and Cl^- is by far the most dominant anion. Day and King (1995) indicated the dominance of Na^+ and Cl^- in the Berg river catchment. For extensive data on the discharge of salts from the Goedertrou catchment via overland flow and interflow, the reader is referred to Jovanovic, Bugan, Frantz, De Clercq and Fey (2008) and De Clercq, Jovanovic and Fey (2010).

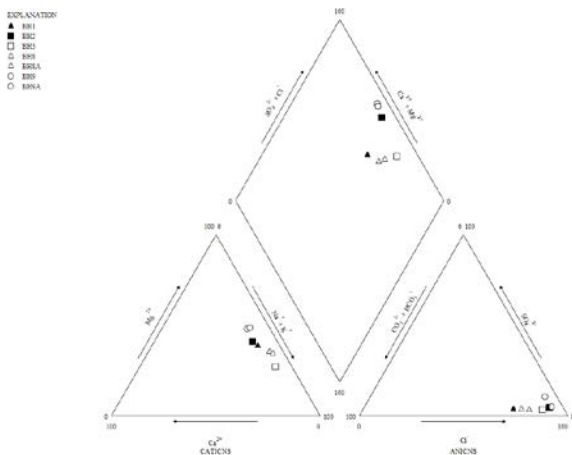


FIG. 9 PIPER DIAGRAM OF GROUNDWATER CHEMISTRY AT GOEDERTROU

Conclusions

This study allowed us to converge on the characterization of regolith salt storage in a small catchment of the Berg river basin through intensive electromagnetic induction and geophysical measurements, as well as borehole information. The regolith in this semi-arid coastal region contains an abundance of stored salts. The regolith in three boreholes showed a sharply peaking concentration of soluble salts between about 5 and 10 m depth, due to the wetting and dissolution combined effects of infiltrating water and rising water table. As a rough estimate, the regolith contains between 186 and 608 t of salts ha^{-1} , stored mainly as a bulge in the unsaturated vadose zone above the water table and below the soil zone, discharging mainly through lateral leaching by groundwater from the phreatic zone.

Flow pathways and mechanisms of salt transport in the small catchment were identified through electromagnetic induction and resistivity measurements. Salinity in the landscape is driven by the toposequence with anti-erosion contours acting as barriers to water and salt fluxes. Presence of highly saline scalds, where the soil B horizon is absent and a very

thin A horizon lies directly on shale, coincides with convex shapes of the hillslope. Areas in the shallow subsurface with very low resistivity correspond to saline soils with high clay content. This is typical of weathered shale. Significantly, weathered areas of the profile correspond to subsurface geological and, in most cases, topographic flow pathways.

The electromagnetic induction data indicated lower soil salinity at the end of the rainy winter season compared to the dry summer season. The impact of salt discharge was therefore lessened by the fact that most of it was released during periods of high flow so that considerable dilution occurred. The salinity hazard was, however, probably magnified seasonally in the Berg river basin by evaporation from the river and storage dams and by more concentrated salt seepage into the lower reaches during periods of low flow and greater water demand.

The factors related to the magnitude and shape of the deep salinity bulge in the vadose zone need to be investigated further since it may hold the key to estimating the quantity of stored salts in the drier regolith of the lower Berg river basin. Different climates, hydrogeological characteristics and land uses may have resulted in different amounts of salt storage in the soils and regolith. Both land use responses and salt storage capacity are key factors for hydrological modelling and catchment management. It will be essential to investigate a variety of land uses and management in order to recommend the most favourable ones in terms of water consumption and salt discharge.

Groundwater quality becomes increasingly saline (mixed cation-chloride-type) from the recharge area towards the bottom end of the catchment. This rate of salt discharge is sensitive to changes in both climate and agricultural practice and the current rate has the potential to persist, to the detriment of water users, for decades at least, if not a century or two. It would therefore make sense to explore ways in which reduced discharge (*i.e.* enhanced storage) can economically be engineered in key parts of the basin.

ACKNOWLEDGMENT

The authors acknowledge the Water Research Commission (Pretoria, South Africa) for funding the research; the Western Cape Office of the Department of Agriculture (Elsenburg, South Africa) for funding the borehole drilling; JJ Myburgh and Brothers for drilling the boreholes.

REFERENCES

- Acworth, R.I. "Investigation of dryland salinity using the electrical image method." *Australian Journal of Soil Research* 37 (1999): 623-636.
- Acworth, R.I., Jankowski, J. "Salt source for dryland salinity – evidence from an upland catchment on the Southern Tablelands of New South Wales." *Australian Journal of Soil Research* 39 (2001): 39-59.
- Angus, J.F., Gault, R.R., Peoples, M.B., Stapper, M., Van Herwaarden, A.F. "Soil water extraction by dryland crops, annual pastures, and lucerne in south-eastern Australia." *Australian Journal of Agricultural Research* 52 (2001): 183-192.
- Bennett, D.L., George, R.J. "Using the EM38 to measure the effect of soil salinity on Eucalyptus globules in south-western Australia." *Agricultural Water Management* 27 (1995): 69-86.
- Brouwer, J., Fitzpatrick, R.W. "Interpretation of morphological features in a salt-affected duplex soil toposequence with an altered soil water regime in western Victoria." *Australian Journal of Soil Research* 40 (2002a): 903-926.
- Brouwer, J., Fitzpatrick, R.W. "Restricting layers, flow paths, and correlation between duration of soil saturation and soil morphological features along a hillslope with an altered soil water regime in western Victoria." *Australian Journal of Soil Research* 40 (2002b): 927-946.
- Brouwer, J., Van De Graaff, R.H.M. "Readjusting the water balance to combat dryland salting in southern Australia: changing the hydrology of a texture contrast soil by deep ripping." *Agricultural Water Management* 14 (1988): 287-298.
- Bussian, A.E. "Electrical conductance in a porous medium." *Geophysics* 48(9) (1983): 1258 – 1268.
- Clarke, C.J., George, R.J., Bell, R.W., Hatton, T.J. "Dryland salinity in south-western Australia: its origins, remedies, and future research directions." *Australian Journal of Soil Research* 40 (2002): 93-113.
- Corwin, D.L., Plant, R.E. "Applications of apparent soil electrical conductivity in precision agriculture." *Computers and Electronics in Agriculture* 46 (2005): 1-10.
- Day, J.A., King, J.M. "Geographical patterns, and their origins, in the dominance of major ions in South African rivers." *South African Journal of Science* 91 (1995): 299-306.
- De Clercq, W.P., Jovanovic, N., Fey, M.V. "Land use impacts on salinity in Western Cape waters." WRC report No. 1503/1/10. Pretoria: Water Research Commission, 2010.
- DWAF. "Hydrology of the Berg River Basin." Department of Water Affairs and Forestry report No. PG000/00/2491. Pretoria: R.R. Berg (Ninham Shand) in association with BKS Inc., 1993.
- DWAF. "National Water Resource Strategy. 1st edn." Available at <http://www.dwaf.gov.za/Documents/Policies/NWRS/Default.htm> [accessed 25 March 2009], 2004.
- Engel, R., McFarlane, D.J., Street, G. "Using geophysics to define recharge and discharge areas associated with saline seeps in south-western Australia." In *Groundwater Recharge*, edited by M. Sharma, 20-40. Rotterdam: Balkema Publishing Company, 1989.
- FAO. "World Reference Base for soil resources." Rome: Food and Agricultural Organization of the United Nations, 1998.
- Fey, M.V., De Clercq, W.P. "Dryland salinity impacts on Western Cape rivers." WRC report No. 1342/1/04. Pretoria: Water Research Commission, 2004.
- Flugel, W.A. "River salination due to dryland agriculture in the Western Cape Province, Republic of South Africa." *Environmental International* 21(5) (1995): 679-686.
- Gorgens, A.H.M., De Clercq, W.P. "Summary of water quality information system and soil quality studies." WRC report No. TT252/05. Pretoria: Water Research Commission, 2005.
- Greiner, R. "Catchment management for dryland salinity control: Model analysis for the Liverpool Plains in New South Wales." *Agricultural Systems* 56(2) (1998): 225-251.
- Hingston, F.J., Gailitis, V. "The geographic variation of salt precipitated over Western Australia." *Australian Journal of Soil Research* 14 (1976): 319-335.
- Hughes, J.D., Khan, S., Crosbie, R.S., Helliwell, S., Michalk, D.L. "Runoff and solute mobilization processes in a semiarid headwater catchment." *Water Resources Research* 43 (2007): 1-15 (W09402).
- Johnson, C.D. "Distribution of environmental chloride in relation to subsurface hydrology." Cited in Peck, A.J., Williamson, D.R. "Hydrology and salinity in the Collie

- River Basin Western Australia." *Journal of Hydrology* 94 (1987): 67–88.
- Jovanovic, N.Z., Bugan, R.D.H., Frantz, G., De Clercq, W.P., Fey, M.V. "Hydrosalinity fluxes in a small scale catchment of the Berg river (South Africa)." In *Water Pollution IX* edited by D. Prats Rico, C.A. Brebbia, Y. Villacampa Esteve Y, 603-612. Southampton: Wit Press, 2008.
- Loke, H. "Rapid 2D and 3D resistivity and IP inversion using the least squares method. RES2DINV v. 3.4 manual." Available at www.geoelectrical.com [accessed 23 March 2009], 2001.
- McArthur, W.M., Churchward, H.M., Hick, P.T. "Landforms and soils of the Murray River catchment area of Western Australia." Land resources and management series No. 3. Canberra: CSIRO, 1977.
- McNeill, J.D. "Electrical conductivity of soil and rocks." Technical note TN-5, Geonics Ltd., Missisauga, Ontario, Canada, Available at <http://www.geonics.com/pdfs/technicalnotes/tn5.pdf> [accessed 26 March 2009], 1980.
- Pannell, D.J., Ewing, M.A. "Managing secondary dryland salinity: Options and challenges." *Agricultural Water Management* 80 (2006): 41–56.
- Pannell, D.J., McFarlane, D.J., Ferdowsian, R. "Rethinking the externality issue for dryland salinity in Western Australia." *The Australian Journal of Agricultural and Resource Economics* 45(3) (2001): 459-475.
- Parsons, R.P. "A South African aquifer system management classification." WRC report No. 77/95. Pretoria: Water Research Commission, 1995.
- Soil Classification Working Group. "Soil classification. A taxonomic system for South Africa." Pretoria: Department of Agricultural Development, 1991.
- Soltau, L.E., Anderson, N.L. "An integrated geophysical survey of groundwater resources, Mamre area, Western Cape Province." *South African Journal of Geology* 109(4) (2006): 433 – 438.
- Stirzaker, R.J., Cook, F.J., Knight, J.H. "Where to plant trees on cropping land for control of dryland salinity: some approximate solutions." *Agricultural Water Management* 39 (1999): 115-133.
- Telford, W.M., Geldart, L.P., Sheriff, R.E. "Applied geophysics." 2nd edn. Cambridge: Press Syndicate of the University of Cambridge, 1990.
- Van Rensburg, L.D., De Clercq, W.P., Barnard, J.H., Du Preez, C.C. "Salinity guidelines for irrigation: Case studies from Water Research Commission projects along the Lower Vaal, Riet, Berg and Breede Rivers." *Water SA* 37(5) (2011): 739-750.